ELSEVIER

Journal of Volcanology and Geothermal Research 98 (2000) 209–217

Journal of volcanology and geothermal research

www.elsevier.nl/locate/jvolgeores

Elastic and fracture parameters of Etna, Stromboli, and Vulcano lava rocks

M. Ciccotti*, N. Negri, L. Sassi, G. Gonzato, F. Mulargia

Dipartimento di Fisica, Settore di Geofisica, Università di Bologna, Viale Berti Pichat 8, 40100 Bologna, Italy

Received 15 October 1998; received in revised form 5 November 1999; accepted 5 November 1999

Abstract

The results of a series of experiments aimed at characterizing the elastic and failure parameters of lava specimens from Mount Etna, Vulcano and Stromboli volcanos is presented. The double torsion—constant configuration—load relaxation method has been employed to obtain the behavior of the stress intensity factor versus mode I subcritical crack velocity. The experimental technique has been optimized in several respects. First, a very stiff machine, expressly designed and built, has been used. Second, all samples have been carefully machined to low tolerance. Third, the experimental conditions have been carefully controlled, with temperature variations within 1°C and humidity within 10%. Fourth, high resolution electronic measuring systems have been used together with a pulse stacking procedure. Fifth, the length of the prefracture has been optically checked. This optimization allowed us to measure the slope of the subcritical fracture propagation curve in the III region, which extends from velocities of 10^{-7} m/s to catastrophic, with a standard deviation around 20%, suggesting that the results can be effectively used for modeling purposes. As a by-product, we could measure the elastic parameters with an accuracy of a few percent.

Keywords: Mount Etna; Vulcano; Stromboli; elastic and fracture parameters; double torsion

1. Introduction

It has been widely acknowledged that fracture is the physical process ruling many geophysical phenomena such as earthquake generation and the onset of volcanic eruptions. Unfortunately, fracture physics is so complex that it has proved so far impossible to develop widely applicable theoretical models. Some models have indeed been developed, but their practical application is tied to the knowledge of fracture parameters, such as the mode I critical stress intensity factor K_{IC} and the subcritical crack growth index n, which is lacking due to the traditional impossibility of acquiring coherent data. We have focused our interest on this specific problem, attempting to improve the existing experimental techniques. Thus, we started from the most reliable experimental procedure for measuring fracture parameters, double torsion at constant configuration, and attempted to improve it. We have apparently been successful.

2. The double torsion testing method

The double torsion—load relaxation—constant configuration method was developed by Evans (1972) to obtain the velocity of crack propagation versus the mode I stress intensity factor. A constant displacement is applied to the specimens through a

* Corresponding author. Fax: +39-51-630-5058.
E-mail address: matteo@ibogeo.df.unibo.it (M. Ciccotti).

0377-0273/00/$ - see front matter
PII: S0377-0273(99)00154-7

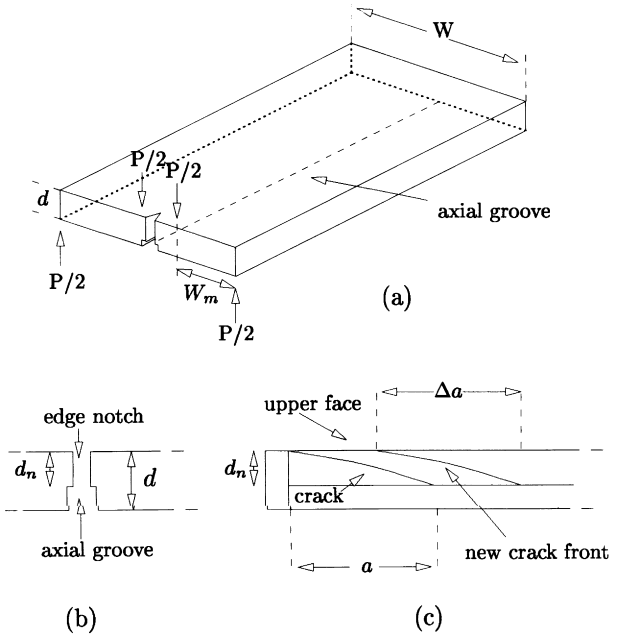

Fig. 1. Sketch of a double torsion specimen configuration: (a) general view; (b) axial cross section; (c) longitudinal cross-section (modified after Atkinson, 1979). The moment arm W_m for our loading machine is fixed at 20 mm.

four point bending scheme as in Fig. 1a. The fracture front proceeds along a straight line starting from a machined initial notch and guided by a side groove thus producing a relaxation of the load.

The method has various advantages, the main of which is its capability to produce stable crack propagation, which makes it very convenient for studying fracture in brittle materials like rocks (Atkinson, 1987). Another advantage of the method is that it only requires one to monitor the decrease of the load with time to measure both the stress intensity factor and the crack velocity, without any need to measure the crack length during the experiment. The mode I stress intensity factor is given by (Williams and Evans 1973):

$$K_I = \sqrt{EG} = PW_m\sqrt{\frac{3(1+\nu)}{Wd^3d_n}} \quad (1)$$

where E is the Young modulus, G the strain energy release rate, P the applied load, W_m the moment arm of the torsion, ν the Poisson's ratio, W the specimen width, d the specimen thickness, and d_n the thickness of the specimen minus the groove depth.

By differentiating the equation of the specimen compliance:

$$C = \frac{y}{P} = \frac{3W_m^2 a}{Wd^3\mu} \quad (2)$$

with a constant displacement assumption we obtain the crack velocity v using the load relaxation data and a single measure of initial (or final) crack length, provided that this is a relatively large fraction of the specimen dimensions (Williams and Evans, 1973):

$$v = -\phi a_{i,f} P_{i,f} \frac{1}{P^2}\frac{dP}{dt} \quad (3)$$

where t is time, a is the crack length and the suffixes i and f denote reference measurements taken either at the beginning or at the end of a test (we used the initial reference in our tests). The factor $\phi = d_n/\sqrt{\Delta a^2 + d_n^2}$ is necessary to balance the effect of the difference Δa in the crack length between the upper and lower face of the specimen (Atkinson, 1987): the crack front is actually diagonal (Fig. 1c), so that its effective normal velocity v equals da/dt reduced

by a factor ϕ. The difference Δa in crack advancement between the upper and lower faces of the specimen has been empirically found to be fixed and equal to five times the thickness d_n in the crack plane.

This approach has been followed by various authors, but the precision achieved so far has been poor, with v vs. K_I curves taken even on the same specimen yielding considerable scatter (Atkinson, 1984; Swanson, 1984).

3. Test material

Our specimens were cut from samples of volcanic rocks extracted from the Mount Etna, Sicily, 1981 flank eruption, from the Punta dello Scoglitto lava flow, from the Fossa latitic eruption, from the Lentia rhyolitic dome, all at Vulcano, Aeolian Islands, and from the shoshonitic basaltic eruption at the Filo del Fuoco in Stromboli, Aeolian Islands. The rocks from Vulcano and Stromboli are all dated between 113 000 years b.p. and the historical epoch (Calanchi et al., 1996). Petrographic analysis shows a homogeneous vesicular porphyritic structure in most of the samples, allowing us to assume isotropic mechanical properties. The porosity is determined by sub-spherical pores of variable dimensions ranging from fractions of a mm to a few mm. The chemical composition of each type of rock is determined by XRF analysis; the percentages of the main oxides are reported in Table 1. The lithotypes are displayed on a TAS diagram (Total-Alkali–Silica) in Fig. 2.

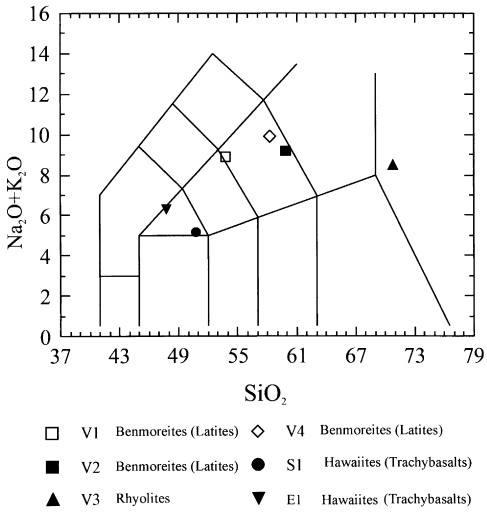

Fig. 2. TAS diagram (Total-Alkali-Silica) for all the lithotypes analyzed. The symbols show the various lithotypes analyzed.

4. Optimizing the experimental technique

We attempted to achieve a better accuracy in measuring the fracture parameters by optimizing several experimental aspects. These were:

- A very sturdy machine, run at a small fraction of its load capability.
- Careful specimen preparation, which included low tolerance machining.
- Tight control of the experimental conditions (temperature and humidity).
- High resolution digital electronics and data processing, which also allowed an improved accuracy in the measured elastic parameters.
- An optical check of the prefracture length.

Table 1
Percentage of major oxides in the specimens (from XRF analysis) normalized to 100 and LOI percentage (Lost Oxides Index). The content of FeO was zero for all rocks except E1, for which it was 6.83%. The different lithotypes analyzed are relative to the Mount Etna, Sicily, 1981 flank eruption (E1), to the Punta dello Scoglitto lava flow (V1), to the Fossa latitic eruption (V2 and V4), to the Lentia rhyolitic dome (V3), all at Vulcano, Aeolian Islands, and to the shoshonitic basaltic rocks at the Filo del Fuoco in Stromboli (S1), Aeolian Islands. The rocks from Vulcano and Stromboli are all dated between 113 000 years b.p. and the historical epoch

Specimen	SiO_2 (%)	TiO_2 (%)	Al_2O_3 (%)	Fe_2O_3 (%)	MnO (%)	MgO (%)	CaO (%)	Na_2O (%)	K_2O (%)	P_2O_5 (%)	LOI (%)
V1	54.13	0.60	17.22	8.12	0.16	3.20	7.20	5.14	3.73	0.49	0.79
V2	59.71	0.47	17.42	6.13	0.13	1.87	4.54	4.17	5.03	0.33	5.29
V3	70.74	0.22	14.21	3.32	0.08	0.66	2.15	3.87	4.62	0.11	0.53
V4	58.19	0.60	18.72	7.06	0.11	1.37	3.70	4.05	5.74	0.46	1.59
S1	51.11	0.86	18.49	8.64	0.17	4.81	10.51	2.82	2.17	0.42	0.1
E1	47.88	1.58	17.74	3.29	0.19	4.73	10.36	4.69	1.53	0.42	0.75

Table 2
The scatter in the P and S wave velocities in each specimen for all directions of propagation is given by the I and III quartile values (in units of 10^3 m/s). The median value of the Poisson's ratio ν is given in the third column. The last column shows the corresponding fracture toughness K_{IC} value. The different lithotypes are given in the caption of Table 1

Specimen	V_p (km/s) I_q–III_q	V_s (km/s) I_q–III_q	ν	K_{IC} (M Nm$^{-3/2}$)
V1	1.44–1.78	0.88–1.04	0.24	0.445
V2	3.05–3.16	1.80–2.13	0.17	1.006
V3	3.48–3.62	1.92–2.26	0.24	1.248
V4	2.30–2.53	1.26–1.69	0.26	0.165
S1	1.86–2.06	1.21–1.39	0.11	0.227
E1	3.31–3.43	1.89–2.15	0.21	1.763

4.1. The loading machine

The machine we used to apply the load is functionally similar to the widely used Instron testing machine and consists essentially of a servo-controlled electric motor which, through a cascade of worm gears, can apply a given displacement to a specimen, while measuring the applied load by a load cell mounted in series with the specimen. Our machine is custom designed and built to maximize stiffness, with a solid stainless steel frame 25.4 mm thick. It was designed for a nominal working load of 20 000 N and, to further guard against frame deformation, it was always used at loads less than 1500 N. Specimens may be up to 20 mm thick and up to 200 mm wide.

4.2. Specimen preparation

Specimens for double torsion testing were machined using a precision diamond head into slabs 200 mm long, 70 mm wide, and with a set of different thickness values ranging between 4.7 and 9.4 mm. A groove with a depth equal to 1/3 the specimen thickness was also machined along one of the faces along with a 10-mm-long, 1-mm-wide edge notch to guarantee a rectilinear propagation of the fractures. The tolerance was always kept within 0.4 mm. We used width to thickness ratios between 8:1 and 15:1, at which Eq. (1) can be shown to be well applicable (Ciccotti, 1999).

4.3. Control of the experimental conditions

Since tiny deformations in the frame of a stiff loading machine can greatly affect the applied load, it is essential that temperature be kept as constant as possible. We used a heat pump and an electronic differential thermostat to keep temperature variations within 1°C in a dedicated room. The variations of humidity, which do not affect the loading machine, but which can affect the fracture properties of the rock, were kept within 10%.

4.4. High resolution electronics

The high resolution achievable through up-to-date electronic devices was beneficial to two different experimental steps. First, the output of the load cell was fed into an analog–digital converter, digitally amplified, and sent via a serial port to a computer workstation where it was recorded, to guarantee the acquisition of massive data sets. Second, since Eq. (1) requires the knowledge of the Poisson's ratio ν, we developed a procedure that used isotropic elastic wave velocities to measure ν:

$$\nu = \frac{\left[\left(\frac{V_p}{V_s}\right)^2 - 2\right]}{2\left[\left(\frac{V_p}{V_s}\right)^2 - 1\right]} \tag{4}$$

Essentially, we used the standard time-of-flight measurement for pulse trains of P and S waves between a sensor and an emitter placed at given positions on the specimen. Step functions with exponential fall were generated by a function generator, pulsed at frequencies varying from 10 Hz to 1 kHz, and injected into the specimen as elastic waves by means of a custom-built piezoelectric transducer, checking in all cases that the frequency value was far from the resonance of the specimen. Time stacking of the recorded signal was then used together with an averaging over 1000 pulses. This allowed an

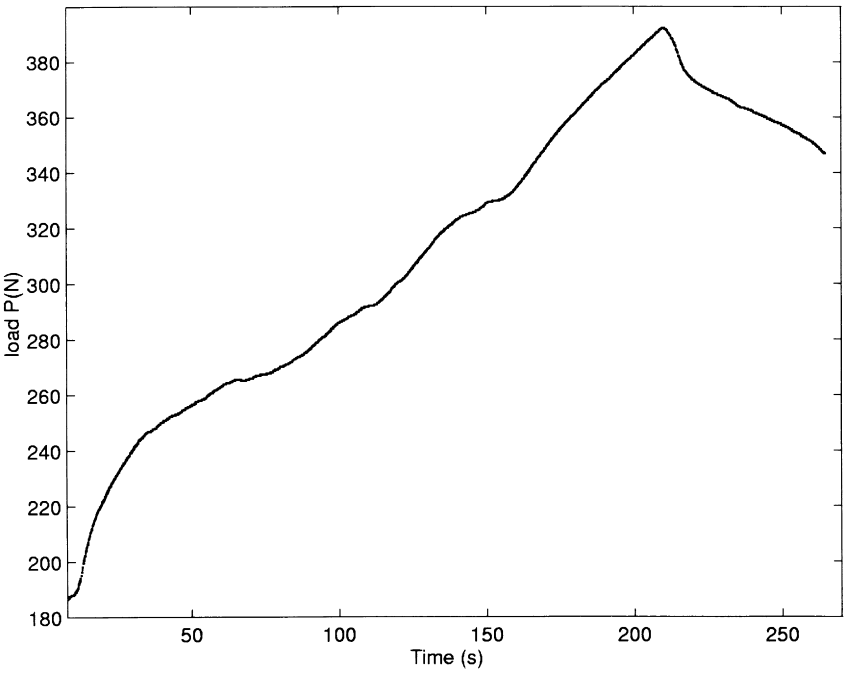

Fig. 3. The load curve in a typical pre-fracture run. The fracture is initiated at ≈ 220 s when a load drop occurs.

improvement in the signal to noise ratio of approximately 20 db.

For each specimen the wave velocities were calculated twice for seven different configurations of the transmitter and receiver, which were glued to the specimen by using cyanoacrilate compounds to ensure good mechanical coupling. The internal scatter of each P and S wave velocity measurement was within a few percent, and also the variation for the different travel paths was limited to about 10% for P waves and 20% for S waves. This indicated a fairly modest anisotropy, which made it possible to apply the isotropic approximation, implemented by taking the median value for each sample. The scatter on the measurements is given by the I and III quartile values of the velocities measured in all directions, which are shown in Table 2 along with the median Poisson's ratio.

4.5. Optical check of the prefracture length

In order to employ Eqs. (1) and (3) it is necessary to create an initial fracture of known length in the specimen. The traditional approach consists, first of all, of cutting a notch of given length along its major axis (see Fig. 1a and b). Since this cut will have a blunt end, while it is necessary to have a sharp fracture, the specimen is loaded at the lowest possible constant strain rate and the load is closely monitored. As soon as a decrease in load is observed, loading is immediately stopped. A typical prefracture load vs. time curve is shown in Fig. 3. It clearly shows the loading at constant rate, followed by a knee. The drop in load is interpreted as the initiation of a fracture, which is nevertheless classically assumed to have propagated for such a short length that it can be disregarded. In light of this, the length of the initial fracture is classically taken to be that of the notch. We checked this by observing the presence of a fracture in the groove (opening side) with an optical stereo microscope. We have in most cases found that a fracture can be quite easily observed and that its length (generally a few centimeters) can never be disregarded. In general, we were also able to observe the final length of the fracture after a relaxation run and this value was cross-checked by integrating the measured velocities of fracture propagation.

The apparatus proved very stable so that several

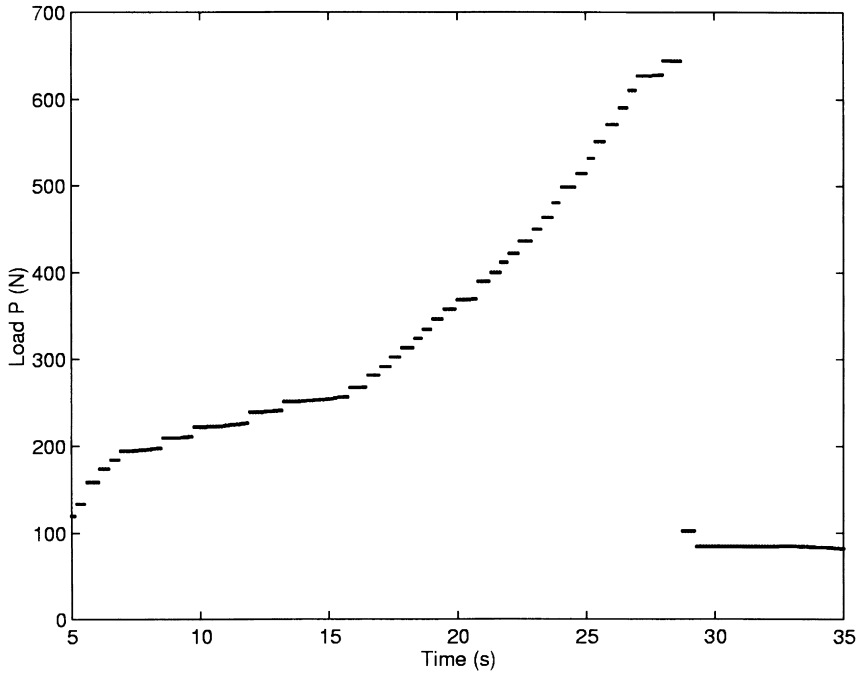

Fig. 4. The general aspect of a critical loading curve consists of a sharp rise of the load followed by an instant drop consequent to the specimen failure.

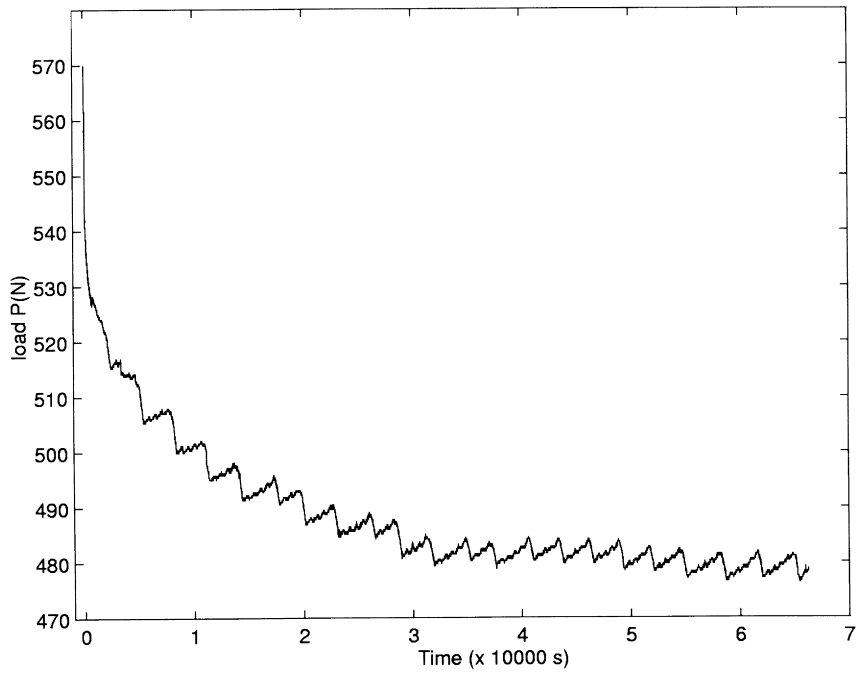

Fig. 5. A typical load relaxation curve. The load fluctuations induced by periodic temperature variations are clearly apparent.

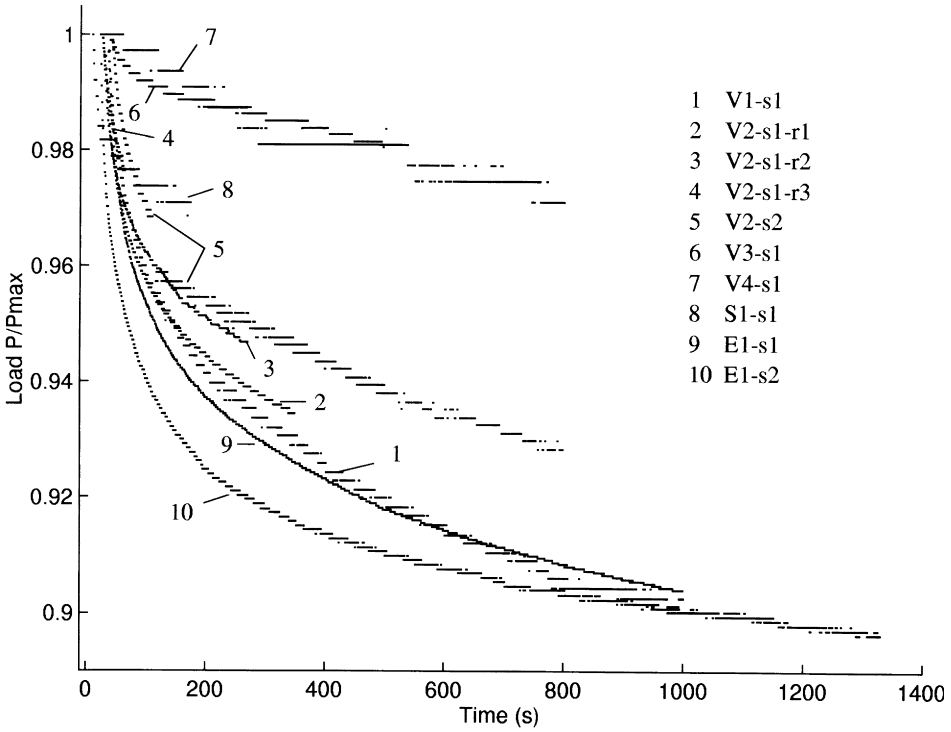

Fig. 6. The initial part of the load relaxation curves, which were used in the analysis, each one normalized to the maximum load P_{max} reached in the run. The label numbers are the same as in Table 3.

relaxation runs could sometimes be performed on the same specimen.

4.6. Determination of fracture toughness K_{IC}

All the measurements of the critical load P_C were performed on pre-fractured specimens. One or more specimens for each lithotype were loaded at the highest possible rate until they broke and the relative K_{IC} was then calculated through Eq. (1) (the median value for each lithotype is reported in Table 2). The loading curves have a general aspect as in Fig. 4, showing that no significant relaxation takes place before the failure. At this point the load relaxation procedure was ready to start.

4.7. Load relaxation

A specimen was loaded at the highest possible rate up to 90–95% of the load relative to K_{IC}, the machine was stopped and the load relaxation with time was recorded.

Table 3
The experimental log exponents of the velocity of fracture propagation versus stress intensity factors in the III regime of the mode I subcritical fracture propagation, for the lithotypes we considered. The different lithotypes are given in the caption of Table 1. Letter 's' denotes different specimens of the same lithotype. Letter 'r' denotes different relaxation tests on the same specimen

	Specimen	*n*
1	V1-s1	25.4
2	V2-s1-r1	49.3
3	V2-s1-r2	61.5
4	V2-s1-r3	47.2
5	V2-s2	36.5
6	V3-s1	125
7	V4-s1	22.6
8	S1-s1	92.1
9	E1-s1	43.1
10	E1-s2	45.9

Load was sampled at 10 Hz for the whole run, which typically lasted 10 h. Only the initial part of load relaxation was actually used (≃1000 s), though, due to the load fluctuations induced by temperature in spite of its tight control, which are apparent when the relaxation rate becomes slow (see Fig. 5 and the discussion below).

5. Results

Sixty-five specimens were cut from a total of 70 kg of lava rocks. A fraction of them had to be discarded because they contained void inclusions large enough to prevent effective measurements. Another fraction accidentally broke during the machining. A further fraction had to be discarded for an insufficient number of samples of identical lithotype.

We measured six different lithotypes, respectively, one coming from Mount Etna volcano, four from Vulcano and one from Stromboli. In spite of the tight control of the environment conditions, the load fluctuation induced by the near periodical temperature variation due to the thermoregulation cycle was generally large (see Fig. 5). We could thus only measure the initial part of the relaxation curve, in which the relaxation rates are high and the load fluctuations induced by temperature variations are comparatively small. Each relaxation curve was therefore analyzed only in the interval preceding the first evident effect of temperature fluctuations (Fig. 6). As a consequence, we could not measure the whole subcritical v vs. K_I curve of mode I fracture propagation, but only its region III, which regards the highest velocities of propagation. This one is actually the most important one for modeling purposes, since it immediately precedes catastrophic propagation. The dependence of v on K_I in region III is a power law:

$$v = AK_I^n \tag{5}$$

where A is a constant and n is the subcritical crack growth index. The experimental results are reported in Fig. 7.

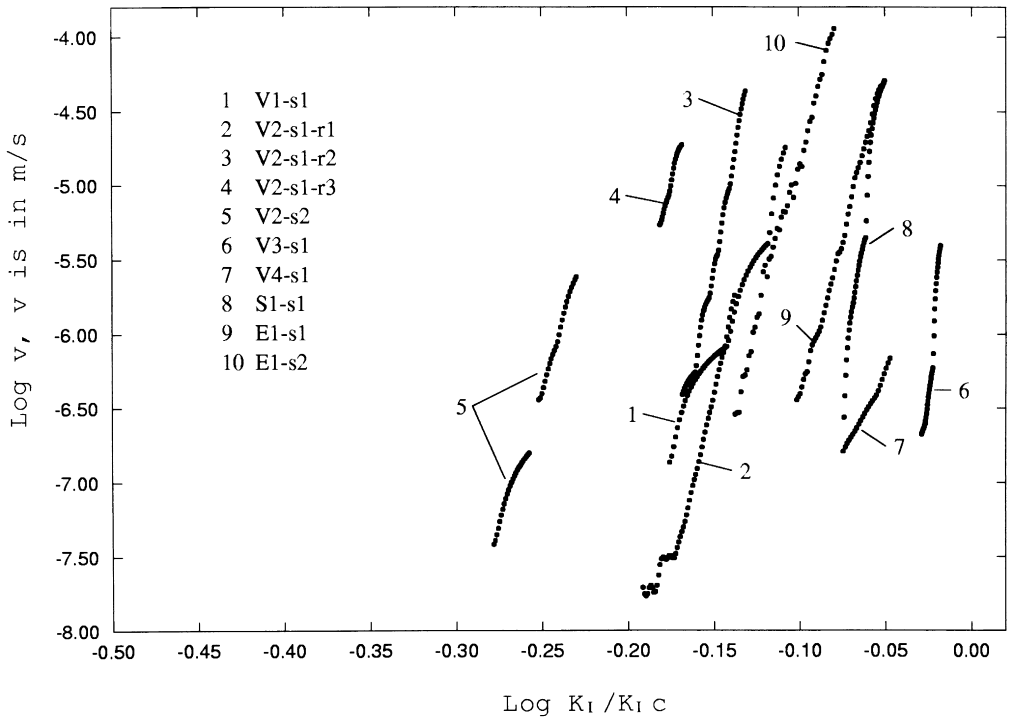

Fig. 7. Region III of the subcritical crack growth curves ($v - K_I$). The stress intensity factor is normalized to the critical value of each lithotype. Notice the coherence and linearity in the slope. The horizontal separation is due to the different values of K_I and is related to the different lithotypes.

The measured velocities of propagation were in the range 10^{-7}–10^{-4} m/s, in which a log-linear relation was found to provide a very good fit to the data ($r^2 \geq 0.90$ in all cases). Since theoretical considerations yield that these slopes remain constant up to the critical value of the stress intensity factor (e.g. Atkinson, 1987), it is possible to calculate the evolution of fracture propagation from velocities of 10^{-7} m/s to catastrophic propagation. The values of the subcritical fracture propagation index n for each lithotype are given in Table 3. Particularly important is the case of the Etna (E1) and Vulcano (V2) lithotypes, for which several independent relaxation runs could be performed, respectively, two for E1 and four for V2. A good coherence was found, with repeatability of the measurement of the region III fracture slope within 20%.

6. Conclusions

While fracture is the physical process ruling many geophysical phenomena, it is so complex that developing theoretical models which can be effectively applied in practice has proved so far to be an impossible task. Furthermore, even the applicability of the models which have been developed has been hampered by the lack of a sufficiently accurate knowledge of fracture parameters. We have focused our interest on this problem, attempting to improve the existing experimental techniques for the measurement of fracture parameters. We started from the most reliable experimental procedure, double torsion at constant configuration, and optimized several experimental aspects. These ranged from mere mechanical features like the stiffness of the loading machine, to the tight control of the environment, to data acquisition and inversion procedures. This optimization has been apparently successful and allowed us to measure the subcritical fracture propagation index n with good coherence and repeatability. The standard deviations of order 20% obtained for this index suggest that it can be effectively used for modeling purposes.

Quite obviously, the reliability of each model will be tied to its assumptions and the incorporation of the present results into a model will have also to satisfy this compatibility.

Acknowledgements

This study was performed with contributions of EEC grant EV-5V-CT 92-0190 and CNR, Gruppo Nazionale per la Vulcanologia. We wish to thank B. Evans and G. Ito for their constructive critiques and M. Bacchetti, who skillfully and patiently machined the specimens.

References

Atkinson, B.K., 1979. Technical note. Int. J. Rock Mech. Min. Sci., Geomech. Abstr. 16, 49–53.

Atkinson, B.K., 1984. Subcritical crack growth in geological materials. J. Geophys. Res. 89, 4077–4114.

Atkinson, B.K., 1987. Fracture Mechanics of Rock. Academic Press, New York.

Calanchi, N., Rossi, P.L., Sanmarchi, F., Tranne, C.A., 1996. Guida escursionistico vulcanologica delle isole Eolie. Centro Studi e Ricerche di Storia e Problemi Eoliani.

Ciccotti, M., in prep. A realistic finite element study for the Double Torsion loading configuration. Submitted for publication.

Evans, A.G., 1972. A method for evaluating the time-dependent failure characteristics of brittle materials—and its applications to polycrystalline alumina. J. Mater. Sci. 7, 1137–1146.

Swanson, P.L., 1984. Subcritical crack growth and other time—and environment—dependent behavior in crustal rocks. Journ. Geoph. Res. B 89 (6), 4137–4152.

Williams, D.P., Evans, A.G., 1973. A simple method for studying slow crack growth. J. Test. Eval. 1, 264–270.